Speed and Current Control of Permanent Magnet Synchronous Motor Drive Using IMC Controllers

Pavel BRANDSTETTER, Tomas KRECEK
VSB - Technical University of Ostrava, 70833, Czech Republic
pavel.brandstetter@vsb.cz

***Abstract*— The paper describes a current and speed control of the permanent magnet synchronous motor with vector control. For a current and speed controller, the Internal Model Control (IMC) method was chosen for its good tracking capability and demands on the controllers. A short analysis of the IMC method for design of the current and speed controller has been made. The paper contains mathematical description of the IMC controller design. Simulation and experimental results of the vector controlled AC drive with interior permanent magnet synchronous motor are shown to present features of the current and speed controller.**

***Index Terms*— permanent magnet synchronous motor, closed loop systems, variable speed drive, vector control, digital signal processor.**

I. INTRODUCTION

Electrical drives with permanent magnet synchronous motors are widely used in industry and transportation. They are an attractive solution for servo drives in the middle power area.

The traditional synchronous machine is one that features an AC winding in the stator that generates a rotary magnetic field in the air gap. The magnetic field of the rotor is generated either by rotor winding that excites electrically with direct current or by permanent magnets. The magnetic field generated by the rotor acts together with the stator field to establish torque on the machine shaft. The speed of the PMSM with constant rotor excitation is determined by the stator frequency and the number of poles. For variable speed drive, some type of inverter is necessary to provide voltage with variable frequency to the permanent magnet synchronous motor [1] - [6].

The properties of a given Permanent Magnet Synchronous Motor (PMSM) depend, for the most part, on the position of the permanent magnets (PM) inside the motor. The PM may be installed in various ways. The basic construction solution of the PMSM is: a) Surface Mounted Permanent Magnet Synchronous Motor - SMPMSM, b) Interior Permanent Magnet Synchronous Motor - IPMSM) [7].

A successful application of vector control is subject to knowing the position of the rotor and, in synchronous machines, the knowledge of the initial position for a problem-free startup. That is the reason why PMSM feature a position sensor that is fitted to the machine shaft.

In recent years, a vector control becomes the common method of driving the PMSM. This method allows usage of the PSMP in same way as DC machine, provides possibility of using the PMSM even at zero speed at nominal torque. Also, with the vector control gives the PMSM better dynamic behavior in compare with the DC machine [8] - [11].

II. LIST OF THE USED SYMBOLS

$\mathbf{u}_{Sdq}$	stator voltage vector in [d, q] coordinate system
$\mathbf{i}_{Sdq}$	stator current vector in [d, q] coordinate system
$\boldsymbol{\psi}_{\mathbf{dq}}$	rotor flux vector in [d, q] coordinate system
$\mathbf{L}_{dq}$	matrix of the stator inductances in [d, q] system
$\mathbf{Z}_{dq}$	matrix of the impedances in [d, q] system
$\mathbf{G}$	system matrix
$\mathbf{I}$	unit matrix
$\mathbf{W}$	cross coupling matrix
$\mathbf{E}$	matrix of the induced voltage
Ψ_{PM}	maximum value of magnetic flux created by PM
R_S	stator resistance
L_S	mean value of the stator inductance
ΔL_S	amplitude of the stator inductance
ΔL	amplitude of the magnetizing inductance
L_d , L_q	stator inductances in [d, q] coordinate system
i_{Sd}, i_{Sq}	stator current vector components in [d, q] system
i_{S_ref}	reference stator current
K_m	gain of the voltage inverter
J_{tot}	total moment of inertia
T_M	driving torque
T_L	load torque
ε	rotor angle
ω_R	rotor angular speed
ω_{m_ref}	reference speed
ω_m	mechanical rotor angular speed

III. MATHEMATICAL MODEL OF THE PMSM

For control purposes, a PMSM model in the rotating coordinate system [d, q] is more suitable. Transformation of PMSM variables into rotor coordinates [d, q] allows implementing vector control which provides the control of the PMSM excitation and electromagnetic torque separately as in DC machine [12] - [15].

In addition, coordinate transformation eliminates dependence of all variables on the position of the rotor, thus facilitating the analysis of the AC drive with individual closed control loops.

The article has been elaborated in the framework of the IT4Innovations Centre of Excellence project, reg. no. CZ.1.05/1.1.00/02.0070 funded by Structural Funds of the European Union and state budget of the Czech Republic and in the framework of the project SP2012/85 which was supported by Student Grant Competition of VSB-TU of Ostrava.

Digital Object Identifier 10.4316/AECE.2012.04001

We can derive a mathematical model of the IPMSM in the rotor coordinates [d, q]:

$$\mathbf{u}_{\mathrm{Sdq}} = \mathbf{L}_{\mathrm{dq}} \frac{d\mathbf{i}_{\mathrm{Sdq}}}{dt} + \mathbf{Z}_{\mathrm{dq}} \mathbf{i}_{\mathrm{Sdq}} + \omega_R \boldsymbol{\Psi}_{\mathrm{dq}} \tag{1}$$

$$\mathbf{L}_{\mathrm{dq}} = \begin{bmatrix} L_d \\ L_q \end{bmatrix}, \ \mathbf{Z}_{\mathrm{dq}} = \begin{bmatrix} R_S & -\omega_R L_q \\ \omega_R L_d & R_S \end{bmatrix}, \ \boldsymbol{\Psi}_{\mathrm{dq}} = \begin{bmatrix} 0 \\ \Psi_{PM} \end{bmatrix} \tag{2}$$

$$L_d = L_S - \Delta L_S, L_q = L_S + \Delta L_S \tag{3}$$

$$T_M = \frac{3}{2} p_p \left[i_{Sq} \Psi_{PM} + i_{Sq} i_{Sd} \left(L_d - L_q \right) \right] \tag{4}$$

$$J_{tot} \frac{d\omega_m}{dt} = T_M - T_L \tag{5}$$

Very efficient control structure for variable speed electric drives is so called cascade structure (see Fig 1). This type of control structure is very popular in practice because of its flexibility.

The control structure consists of control loops, whereas the current (torque) control loop is subordinate and the speed control loop is superior loop. The cascade control requires a frequency separation of all control loops in the controlled system.

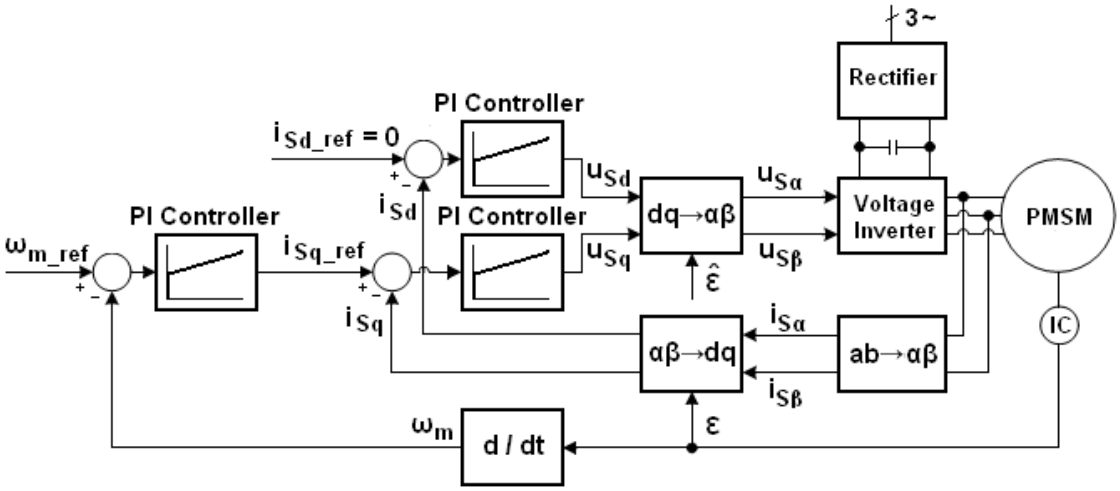

Figure 1. Control structure of the AC drive with the PMSM

IV. Current Control

The current control loop plays a critical role in the overall structure of the vector control. The reason is that the design of superior mechanical systems (velocity and position control loop) assumes its ideal behavior (precise control without delay). Using subordinate current control loop we ensure a quick response to its reference value, which comes from the superior speed control loop. Thus we ensure maximum machine dynamics during sudden change of the desired speed or the desired position. The next task of the current control loop is to keep the current within safe limits and provide precisely decoupled control loops for magnetizing and torque current components i_{Sd}, i_{Sq}.

The main reason why the stator current must not exceed its maximum is the demagnetization of permanent magnets of the machine.

The design of the current controllers for d-axis and q-axis assumes that current changes are much faster than mechanical changes. The behavior of the circuit is described by equation (1), which can be rewritten in the frequency domain in the form:

$$\mathbf{U}_{\mathrm{Sdq}} = \mathbf{G}\, \mathbf{I}_{\mathrm{Sdq}} + \mathbf{W}\, \mathbf{I}_{\mathrm{Sdq}} + \mathbf{E} \tag{6}$$

$$\mathbf{G} = \begin{bmatrix} \dfrac{1}{R_S + sL_d} & 0 \\ 0 & \dfrac{1}{R_S + sL_q} \end{bmatrix} \tag{7}$$

$$\mathbf{W} = \begin{bmatrix} 0 & -\omega_R L_q \\ \omega_R L_d & 0 \end{bmatrix}, \ \mathbf{E} = \omega_R \begin{bmatrix} 0 \\ \Psi_{PM} \end{bmatrix} \tag{8}$$

For clarity, it is true that $\mathbf{U}_{\mathrm{Sdq(s)}} = \mathbf{U}_{\mathrm{Sdq}}$, $\mathbf{I}_{\mathrm{Sdq(s)}} = \mathbf{I}_{\mathrm{Sdq}}$.

The electrical system can be represented as block (see figure 2).

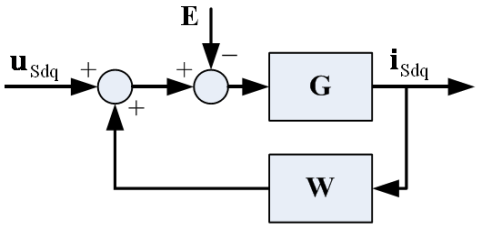

Figure 2. Voltage equation represented in block diagram

Decoupling is the first step in the design of the current controllers and is performed using the following equation:

$$\mathbf{u}_{\mathrm{Sdq}} = \mathbf{u}'_{\mathrm{Sdq}} - \mathbf{i}_{\mathrm{Sdq}} (\mathbf{W} - \mathbf{R}_{\mathrm{a}}) \tag{9}$$

where $\mathbf{R}_{\mathrm{a}} = diag(R_{ad}, R_{aq})$ is so called active damping (also active resistance), which is added to reduce the influence of the disturbance **E** [16]. The resulting electrical system after decoupling using equation (9) is shown in figure 3.

Many methods can be used for the design of current controllers. The Internal Model Control (IMC) method,

which we used for the design of the controllers, has advantageous properties for use in controlled AC drives [16], [17].

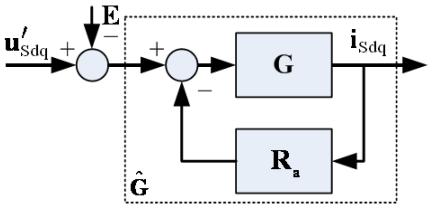

Figure 3. Block diagram of the voltage equation for decoupling and implementation of active damping

The basic idea of the IMC method is that the feedback contains only information about disturbances and errors between the real system and its model.

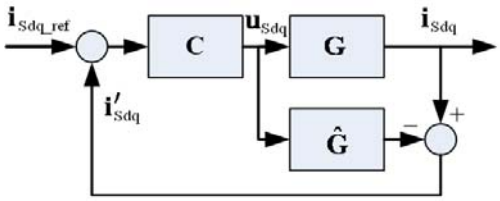

Figure 4. Schematic structure of the IMC

The principle is shown in Figure 4, where **G** is a real system (in this case PMSM) and $\hat{\mathbf{G}}$ is the first-order system see figure 3). We can choose for such system:

$$\mathbf{C} = \hat{\mathbf{G}}^{-1}\mathbf{L} \tag{10}$$

$$\mathbf{L} = diag\left(\frac{\alpha_c}{s+\alpha_c}, \frac{\alpha_c}{s+\alpha_c}\right) \tag{11}$$

α_c is an optional parameter.

Of course, it is not possible to realize the structure in figure 4, since $\hat{\mathbf{G}}$ is not exactly known. But it can be realized classical feedback structure from figure 5.

Based on the analysis of the structure in Figure 4, we can write equation:

$$\begin{aligned}
&\mathbf{C}\left(\mathbf{i}_{\mathrm{Sdq_ref}} - \mathbf{i}'_{\mathrm{Sdq}}\right) = \mathbf{u}_{\mathrm{Sdq}},\\
&\mathbf{C}\left(\mathbf{i}_{\mathrm{Sdq_ref}} - \left(\mathbf{G}\mathbf{u}_{\mathrm{Sdq}} - \hat{\mathbf{G}}\mathbf{u}_{\mathrm{Sdq}}\right)\right) = \mathbf{u}_{\mathrm{Sdq}},\\
&\mathbf{C}\left(\mathbf{i}_{\mathrm{Sdq_ref}} - \left(\mathbf{G}\mathbf{G}^{-1}\mathbf{i}_{\mathrm{Sdq}} + \hat{\mathbf{G}}\mathbf{u}_{\mathrm{Sdq}}\right)\right) = \mathbf{u}_{\mathrm{Sdq}},\\
&\mathbf{C}\mathbf{i}_{\mathrm{Sdq_ref}} - \mathbf{C}\mathbf{i}_{\mathrm{Sdq}} + \mathbf{C}\hat{\mathbf{G}}\mathbf{u}_{\mathrm{Sdq}} = \mathbf{u}_{\mathrm{Sdq}},\\
&\mathbf{C}\left(\mathbf{i}_{\mathrm{Sdq_ref}} - \mathbf{i}_{\mathrm{Sdq}}\right) = \mathbf{u}_{\mathrm{Sdq}} - \mathbf{C}\hat{\mathbf{G}}\mathbf{u}_{\mathrm{Sdq}},\\
&\mathbf{u}_{\mathrm{Sdq}} = \left(\mathbf{I} - \mathbf{C}\hat{\mathbf{G}}\right)^{-1}\mathbf{C}\left(\mathbf{i}_{\mathrm{Sdq_ref}} - \mathbf{i}_{\mathrm{Sdq}}\right).
\end{aligned} \tag{12}$$

where $\mathbf{i}'_{\mathrm{Sdq}}$ is an auxiliary variable and **I** is the unit matrix.

Based on the analysis of the structure in Figure 5, we can write equation:

$$\mathbf{u}'_{\mathrm{Sdq}} = \mathbf{F}\left(\mathbf{i}_{\mathrm{Sdq\_ref}} - \mathbf{i}_{\mathrm{Sdq}}\right) \tag{13}$$

where **E** = 0.

Comparing the equation (13) with equation (12), it can be concluded that the IMC controller **C** can be realized by classical controller **F** which is described as follows:

$$\begin{aligned}
\mathbf{F} &= \left(\mathbf{I} - \mathbf{C}\hat{\mathbf{G}}\right)^{-1}\mathbf{C} = \frac{\alpha_c}{s}\begin{bmatrix} R_s + R_{ad} + sL_d & 0 \\ 0 & R_s + R_{aq} + sL_q \end{bmatrix}\\
&= \frac{\alpha_c}{s}\hat{\mathbf{G}}^{-1}.
\end{aligned} \tag{14}$$

The equations (14), (15) show that the regulator **F** consists of two PI controllers for currents in the d-axis and q-axis.

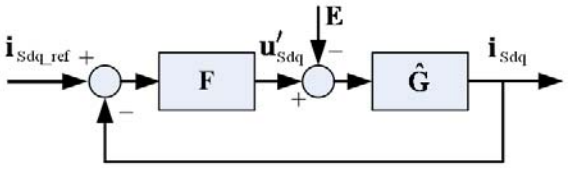

Figure 5. Classical feedback structure

The expression for the transfer function of the closed loop can be written in the form:

$$\mathbf{G}_{\mathrm{w}} = \left(\mathbf{I} + \hat{\mathbf{G}}\mathbf{F}\right)^{-1}\hat{\mathbf{G}}\mathbf{F} = \begin{bmatrix} \frac{\alpha_c}{\alpha_c + s} & 0 \\ 0 & \frac{\alpha_c}{\alpha_c + s} \end{bmatrix} \tag{15}$$

The closed loop transfer function shows that the closed system is composed of two independent and stable first-order systems with negative real poles $s = -\alpha_c$.

According to the theory, we can write for the rise time of the first-order system $t_r = ln(9)/\alpha_c$. This means, that an optional parameter α_c specifies the desired rise time t_r of the controlled variable, and thus represents the bandwidth of the system.

Now the question arises how to select the active damping $\mathbf{R}_a$. The active damping $\mathbf{R}_a$ reduces effect of disturbances **E**. If this technique is not used, then the active damping will be $\mathbf{R}_a = 0$.

We can derive the transfer function of the controllers from the equation (14):

$$\mathbf{G}_{\mathrm{PIc}} = \begin{bmatrix} K_{pd} + \frac{K_{id}}{s} & 0 \\ 0 & K_{pq} + \frac{K_{iq}}{s} \end{bmatrix} = \begin{bmatrix} \frac{\alpha_c L_d}{K_m} + \frac{\frac{\alpha_c R_s}{K_m}}{s} & 0 \\ 0 & \frac{\alpha_c L_q}{K_m} + \frac{\frac{\alpha_c R_s}{K_m}}{s} \end{bmatrix} \tag{16}$$

where K_m is gain of the voltage inverter.

The control structure from figure 5 can be represented by the equation:

$$\mathbf{i}_{\mathrm{Sdq}} = \left(\mathbf{I} + \hat{\mathbf{G}}\mathbf{F}\right)^{-1}\hat{\mathbf{G}}\mathbf{F}\mathbf{i}_{\mathrm{Sdq\_ref}} - \left(\mathbf{I} + \hat{\mathbf{G}}\mathbf{F}\right)^{-1}\hat{\mathbf{G}}\mathbf{E} \tag{17}$$

where the second term on the right side of the equation represents a transfer function of disturbances.

We can derive the transfer function of disturbances:

$$\mathbf{G}_u = \left(\mathbf{I} + \hat{\mathbf{G}}\mathbf{F}\right)^{-1}\hat{\mathbf{G}} = \begin{bmatrix} \frac{s}{(s+\alpha_c)(sL_d+R_s+R_{ad})} & 0 \\ 0 & \frac{s}{(s+\alpha_c)(sL_q+R_s+R_{aq})} \end{bmatrix} \quad (18)$$

If we choose:

$$\mathbf{R}_a = diag(\alpha_c L_d - R_s, \alpha_c L_q - R_s), \quad (19)$$

then the transfer function of disturbances is changed in the following form:

$$\mathbf{G}_u = diag\left(\frac{s}{L_d(s+\alpha_c)^2}, \frac{s}{L_q(s+\alpha_c)^2}\right). \quad (20)$$

The result is a double pole of the disturbance transfer $s = -\alpha_c$, thus the disturbances transfer is fast as transfer of the closed loop $\mathbf{G}_w$, which has a simple pole $s = -\alpha_c$.

Now we perform a small recapitulation. The parameters of the controller are described by equations ($\mathbf{R}_a = 0$):

$$\begin{aligned} K_{pd} &= \frac{\alpha_c L_d}{K_m}, K_{id} = \frac{\alpha_c R_s}{K_m}, \\ K_{pq} &= \frac{\alpha_c L_q}{K_m}, K_{iq} = \frac{\alpha_c R_s}{K_m}, \end{aligned} \quad (21)$$

The controller has a classical PI structure and includes the block of decoupling. Using the active damping $\mathbf{R}_a$ for fast removing the effects of disturbances, we can write for the controller parameters:

$$\begin{aligned} K_{pd} &= \frac{\alpha_c L_d}{K_m}, K_{id} = \frac{\alpha_c^2 L_d}{K_m}, R_{ad} = \frac{\alpha_c L_d - R_s}{K_m}, \\ K_{pq} &= \frac{\alpha_c L_q}{K_m}, K_{iq} = \frac{\alpha_c^2 L_q}{K_m}, R_{aq} = \frac{\alpha_c L_q - R_s}{K_m}, \end{aligned} \quad (22)$$

The structure of the controller is shown in Figure 6, where $\mathbf{K}_p = diag(K_{pd}, K_{pq})$, $\mathbf{K}_i = diag(K_{id}, K_{iq})$ *a* $\mathbf{R}_a = diag(R_{ad}, R_{aq})$.

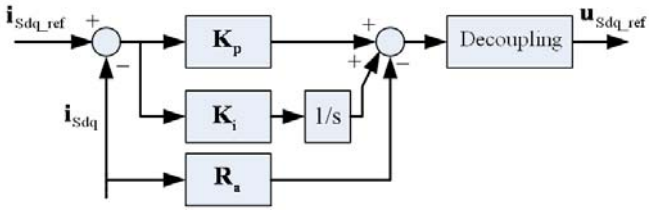

Figure 6. Controller structure with active damping

V. Simulation and Experimental Verification of Current Control Loop

The theoretical assumptions were first verified using computer simulations by software product MATLAB-SIMULINK and subsequently verified experimentally.

The figure 7 shows the controller response with standard technique of decoupling at desired rise time $t_r = 2$ *ms* and with machine parameters listed in the chapter VIII.

We can see that the torque current component i_{Sq} (and thus also the electromagnetic torque of the machine) is controlled very quickly, accurately and without overshoot. Also, both components of the stator current are without significant relationships.

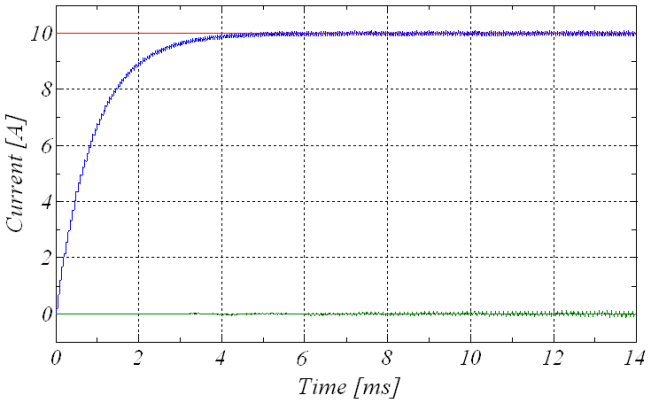

Figure 7. Simulation of current controller response to a step change in the reference quantity i_{Sq_ref}, reference current components $i_{Sq\_ref} = 10$ *A* (red), $i_{Sd\_ref} = 0$ *A*, real current components i_{Sd} (blue), i_{Sq} (green)

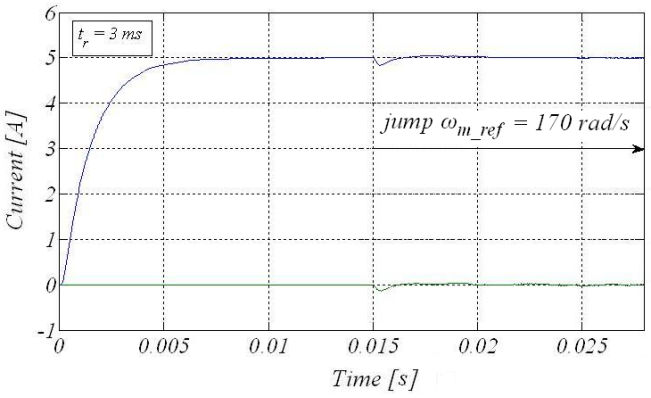

Figure 8. Simulation of current controller response to a step change in the reference quantity ω_{m_ref}, real current components i_{Sd} (blue), i_{Sq} (green)

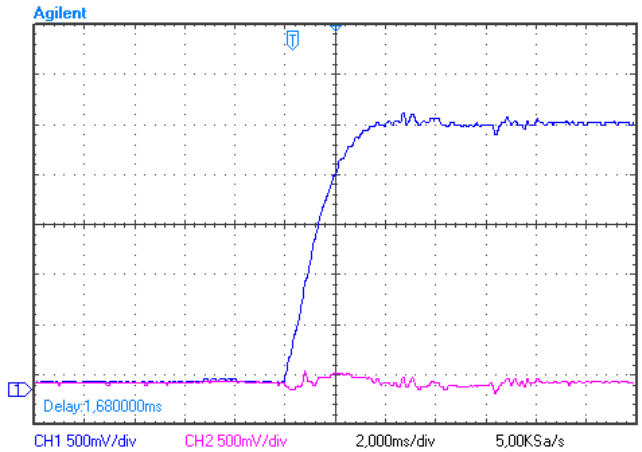

Figure 9. Current controller response to a step change in the reference quantity i_{Sq_ref}, reference current components $i_{Sq\_ref} = 10$ *A*, $i_{Sd\_ref} = 0$ *A*, real current components i_{Sd} (blue), i_{Sq} (red), $m_i = 2$ *A/div*

An important feature of the controller is its behavior to jump of the disturbance. Such behavior of the controller with proposed IMC method with active damping is shown in figure 8. The disturbance is controlled very quickly, accurately and without overshoot. The next step to verify the described theory is an experimental verification on a real drive. The figure 9 shows current controller response to a step change in the reference quantity i_{Sq_ref}. The desired rise time was chosen $t_r = 2\ ms$.

The figure 10 shows the time course of two stator current components i_{Sd}, i_{Sq} at the reversal request (and thus also the torque reversal). The desired rise time was chosen the same $t_r = 2\ ms$. It is evident that the behavior of the real current control loops coincides very well with the theoretical assumptions and simulation results.

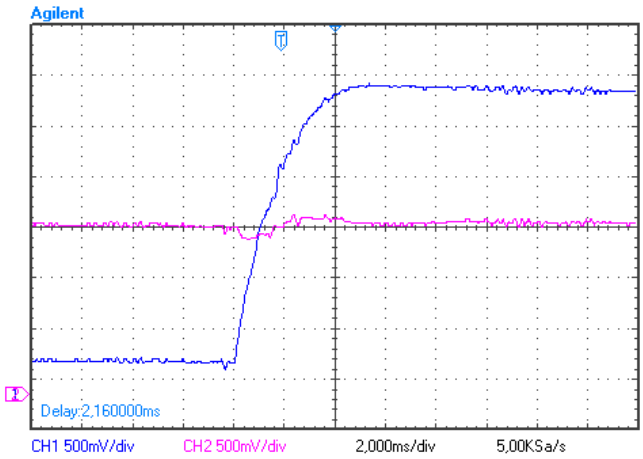

Figure 10. Current controller response to a step change in the reference quantity i_{Sq_ref}, reference current components i_{Sq_ref} = *-10 A → 10 A*, i_{Sd_ref} = *0 A,* real current components i_{Sd} (blue), i_{Sq} (red), m_i = *4,34 A/div*

The result showed the effect of cross coupling in dynamic conditions. However, the current peak does not exceed the value 700 mA. It is necessary to remark that the technique of decoupling (adding terms $-L_q\omega_r i_q$ and $L_d\omega_r i_q$ to the outputs of the controllers) is not fully exact. On the contrary the predicted rise time $t_r = 2\ ms$ agrees quite accurately with the real measured time.

VI. Speed Control

Speed control can be realized by closing the speed loop, encompassing the current control loop as shown in the figure 1.

The torque current component is derived from superior speed control loop. Also the speed control loop uses PI controller for zero steady-state error between the reference and the actual quantity. To create a feedback is necessary to use a mechanical speed or position sensor. At sensorless control, these sensors are represented by the estimated feedback variables of speed and position resulting in the elimination of the mechanical sensor [18]-[23].

The high bandwidth of the current control loop allows the design of the speed controller with neglecting its dynamics and design can only be done by the kinetic equation:

$$\frac{d\omega_m}{dt} = \frac{1}{J_{tot}}\left(T_e - T_z - \omega_m B\right) = \frac{1}{J_{tot}}\left(\underbrace{\tfrac{3}{2}\Psi_{PM}\, p_p}_{K_t}\, i_{Sq} - T_z - \omega_m B\right), \tag{23}$$

For the design of the structure and parameters of the controller, we can use the IMC method. The transfer of the system is described as follows:

$$G_{ss}(s) = \frac{\omega_m(s)}{i_{Sq}(s)} = \frac{K_t}{J_{tot}s + B}. \tag{24}$$

From equation (24), we can derive for the controller transfer:

$$G_{PI_\omega}(s) = \frac{\alpha_s}{s}G_{ss}^{-1} = \frac{\alpha_s}{s}\frac{J_{tot}s + B}{K_t} = K_{p\omega} + \frac{K_{i\omega}}{s} = \frac{\alpha_s J_{tot}}{K_t} + \frac{\frac{\alpha_s B}{K_t}}{s}. \tag{25}$$

How it can be seen, to calculate the gain of the integral component, it is necessary to know the coefficient of friction B. It is very difficult to obtain this parameter, which changes also within operation of the drive. Therefore, we use so called damping coefficient B_a as follows [24]:

$$i_{Sq}^{*} = i_{Sq}'^{*} - B_a\omega_m. \tag{26}$$

Now we can express the system transfer:

$$G_{ss}'(s) = \frac{\omega_m(s)}{i_{Sq}'^{*}(s)} = \frac{\frac{K_t}{J_{tot}}}{s + \underbrace{\frac{K_t B_a}{J_{tot}} + \frac{B}{J_{tot}}}_{\alpha_s}}. \tag{27}$$

It was chosen for simplification in equation (27):

$$\alpha_s = \frac{K_t B_a}{J_{tot}} + \frac{B}{J_{tot}} \Rightarrow B_a = \left.\frac{\alpha_s J_{tot} - B}{K_t}\right|_{\alpha_s J_{tot} \gg B} \approx \frac{\alpha_s J_{tot}}{K_t}. \tag{28}$$

Substituting damping coefficient B_a from equation (28) into (27) we obtain the system transfer:

$$G_{ss}'(s) = \frac{\omega_m(s)}{i_{Sq}'^{*}(s)} = \frac{\frac{K_t}{J_{tot}}}{s + \frac{K_t\left(\frac{\alpha_s J_{tot} - B}{K_t}\right)}{J_{tot}} + \frac{B}{J_{tot}}} = \frac{K_t}{J_{tot}s + \alpha_s J_{tot}}. \tag{29}$$

The final transfer of the control derived from the equation (14) is described as follows:

$$\begin{aligned} G_{PI_\omega}(s) &= \frac{\alpha_s}{s}G_{ss}'^{-1} = \frac{\alpha_s}{s}\frac{J_{tot}s + \alpha_s J_{tot}}{K_t} = \\ &= K_{p\omega} + \frac{K_{i\omega}}{s} = \frac{\alpha_s J_{tot}}{K_t} + \frac{\frac{\alpha_s^2 J_{tot}}{K_t}}{s} \text{ při } B_a = \frac{\alpha_s J_{tot}}{K_t}. \end{aligned} \tag{30}$$

At the end of the chapter is again a small recap. If we have the available friction coefficient B, we can calculate the controller parameters as follows:

$$K_{p\omega} = \frac{\alpha_s J_{tot}}{K_t}, K_{i\omega} = \frac{\alpha_s B}{K_t}, \tag{31}$$

The controller has the classical PI structure. If accurate information of the friction coefficient B is not available, then the controller parameters can be computed according to the relations:

$$K_{p\omega} = \frac{\alpha_s J_{tot}}{K_t}, K_{i\omega} = \frac{\alpha_s^2 J_{tot}}{K_t}, B_a = \frac{\alpha_s J_{tot}}{K_t}, \qquad (32)$$

The speed controller has the structure according the figure 6. The difference is that the current is replaced by the speed and the block of decoupling is not included.

The total transfer of the system (control transfer and disturbance transfer) is then given for the controller with active damping by following equation:

$$\omega_m(s) = \frac{\alpha_s}{s+\alpha_s}\omega_{m\_ref}(s) + \frac{-s}{J_{tot}(s+\alpha_s)^2}T_z(s). \qquad (33)$$

It is obvious that the sensitivity to disturbance (sudden change of load torque) is again significantly better than the standard structure with PI controller. The reason is double pole of the characteristic polynomial.

VII. Simulation and Experimental Verification of Speed Control Loop

The designed structure of the speed controller was first verified using software product MATLAB-SIMULINK and subsequently verified experimentally [25].

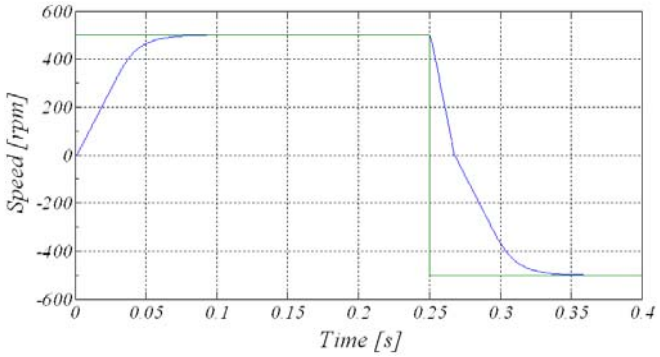

Figure 11. Simulation of speed controller response to a step change in the reference quantity ω_{m_ref}, reference speed $\omega_{m\_ref} = 0 \rightarrow +500$ *rpm* $\rightarrow$ *- 500 rpm* (green), real quantity ω_m (blue)

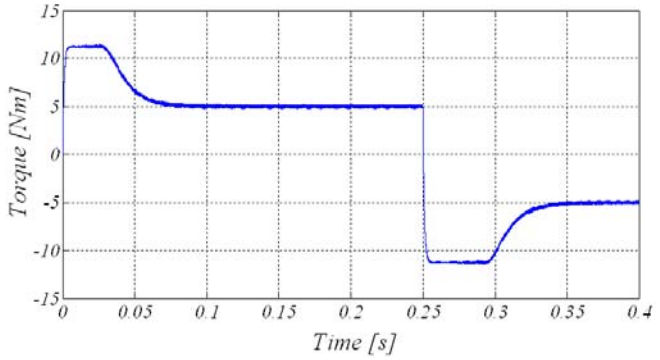

Figure 12. Simulation of speed controller response to a step change in the reference quantity ω_{m_ref}, motor torque T_M (blue)

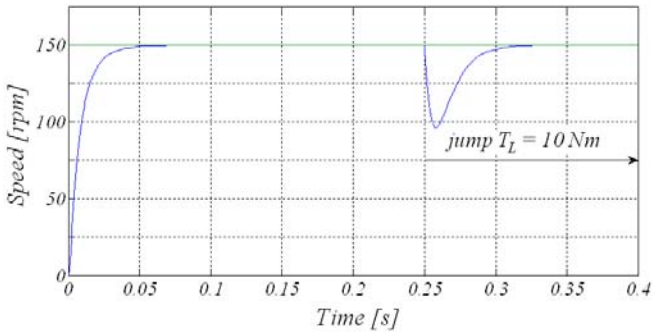

Figure 13. Simulation of speed controller response to a step change in the load torque T_L, reference quantity ω_{m_ref} = *150 rpm* (green), real quantity ω_m= *150 rpm* (blue)

For smooth operation of the cascade control structure is necessary for the current loop bandwidth α_c that it is at least 5 times to 10 times greater than the bandwidth of the speed loop α_s (α_c=*(5~10)* α_s).

The speed response of the control structure according to figure 1 with controllers designed by IMC method and given machine parameters is shown in figure 11.

The time course has nearly zero steady-state error and no overshoot. The figure 12 shows the time course of the motor torque during transient action.

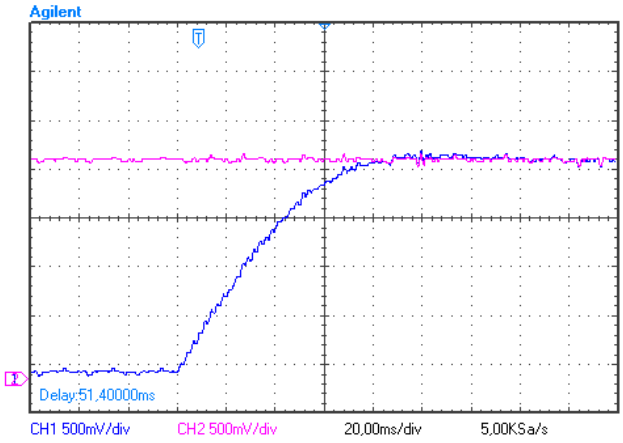

Figure 14. Speed controller response to a step change in the reference quantity ω_{m_ref} (red), reference speed ω_{m_ref} = *0* $\rightarrow$ *1000 rpm* (blue), m_ω = *238 rpm/div*

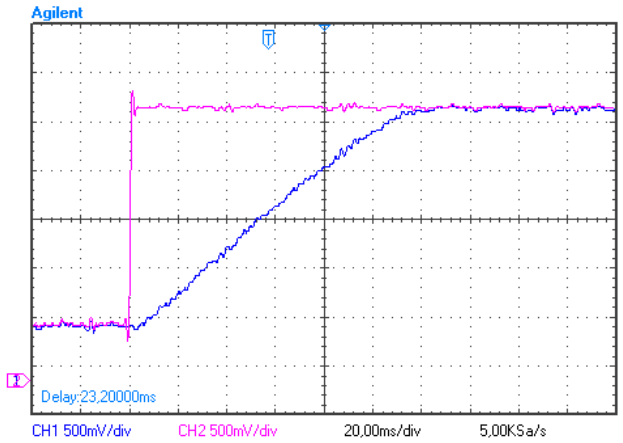

Figure 15. Speed controller response to a step change in the reference quantity ω_{m_ref} (red), reference speed ω_{m_ref} = *-1000* $\rightarrow$ *1000 rpm* (blue), m_ω = *476,2 rpm/div*

An important property necessary for assessing the performance of the vector controlled AC drive is its behavior with the load changes (see figure 13). We can see that the disturbance is controlled as fast and without overshoot.

The experimental verification of speed control loop during acceleration and speed reversal is shown in the figure 14 and 15. The desired rise time was chosen $t_r = 50\ ms$. The time courses of the speed have very good accordance with the theoretical assumptions and simulation results.

In conclusion, it should be noted that each controller is limited on its output and equipped with so called the antiwind-up effect.

VIII. Experimental Laboratory Workplace

The laboratory system consists of an electrical drive, DSP control system and measuring equipment. The mechanical part of the drive contains the IPMSM and a loading induction motor. The IPMSM uses an incremental sensor with 2048 pulses per revolution.

In the control system, a Freescale DSP 56F8037 digital signal processor is used. The base board with the DSP also contains a transducer of the serial line to USB; therefore, communication and data acquisition uses the USB interface. The program is loaded and tuned via the USB interface with a USB TAP by Freescale.

The described control algorithms were simulated by MATLAB-SIMULINK on the vector controlled AC drive with the IPMSM. The controllers of quantities in the control structure of the AC drive were adjusted accordance with the following parameters of the used IPMSM:

- Nominal power $P_n = 2.42$ kW
- Nominal torque $T_n = 7.7$ Nm
- Nominal current $I_{Sn} = 5.65$ A
- Maximal demagnetizing current $I_{Sd} = 26$ A
- Nominal speed $\omega_n = 3000$ rpm
- Number of magnetic pole pairs $pp = 2$
- Nominal power $P_n = 2.42$ kW
- Voltage constant $C_V = 0.7$ V/rad
- Longitudinal inductance $L_d = 1.75$ mH
- Transverse inductance $L_q = 4.9$ mH
- Stator resistance $R_S = 1.11\ \Omega$
- Moment of inertia $J_i = 17.41$ kgcm^2

IX. Experimental Results

In this chapter, the experimental results from measurements on the real AC drive with the vector control of the IPMSM at the speed control are listed. These measurements are performed using a DSP Freescale and application program Freemaster. In each period (100 microseconds) or its multiple is the desired value stored in memory and then retrieved using Freemaster. This procedure is very useful in developing algorithms and analyzing the results. The reasons for such solution are only two D/A converters contained in the DSP and limiting their resolution to 12 bits. To view more than two time courses, the courses will be processed using this procedure. The figures 16-19 show the experimental results of the vector control of the IPMSM using IMC controllers which were measured on the experimental laboratory stand [25].

Thanks to the used IMC controllers, the entire AC drive is stable and it has good dynamics and accuracy.

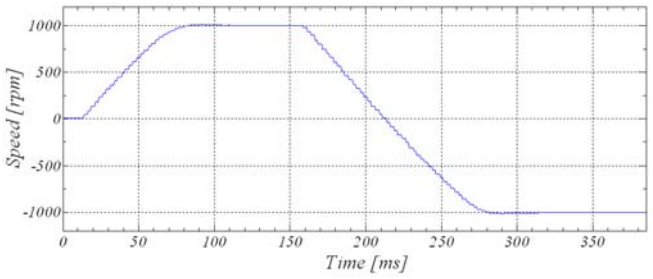

Figure 16. Time response of the motor speed ω_m (blue), reference speed $\omega_{m\_ref} = 0 \rightarrow +1000\ rpm \rightarrow -1000\ rpm$

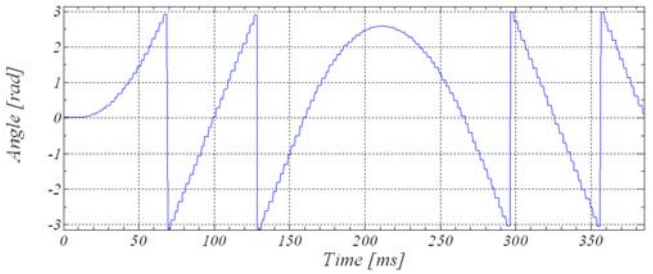

Figure 17. Time response of the rotor angle ε (blue)

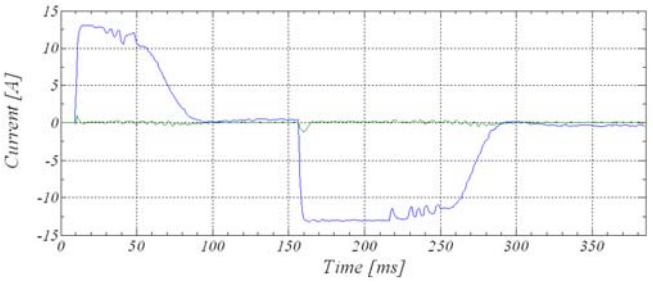

Figure 18. Time response of the magnetizing current component i_{Sd} (green) and torque current component i_{Sq} (blue)

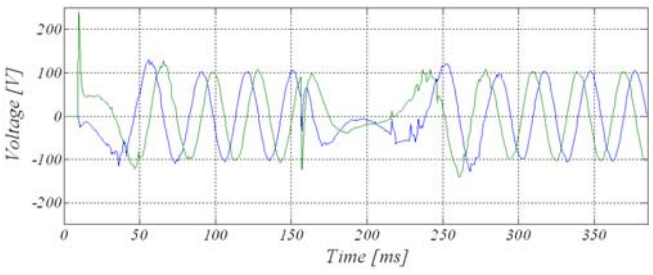

Figure 19. Time response of the stator voltage component $u_{S\alpha}$ (green) and stator voltage component $u_{S\beta}$ (blue)

X. Conclusion

The paper deals with the design of the controllers which are necessary for the vector control structure of the IPMSM. To select an appropriate method for controller design, it is necessary to define the basic requirements, for example the speed control range, the accuracy of the current or speed controls, etc. Only practical verification on laboratory models or in practice determines clearly the suitability of the chosen method. For the controller parameters design, the IMC method was used which is described in the paper.

The described control methods were simulated using

software Matlab-Simulink and then validated on the laboratory model of the AC drive with permanent magnet synchronous motor. If we compare the simulation results with experimental results, we can clearly state that the waveforms controlled variables, it means speed, torque and magnetizing component of the stator current vector are almost identical and express the good correspondence of the theory, simulation and experiments.

The controller parameters had to be fine-tuned due to inaccurate determination of machine parameters by the manufacturer. The controller parameters were not changed more than ±20% of the theoretical value.

The presented method has several advantages: (*a*) result of the procedure is very fast and accurate transient without overshoot, (*b*) very simple design in which only the parameters of the controlled system (R_s, L_d, and L_q) and desired rise time of the controlled variable t_r enter.

For the development of the modern control techniques for AC drives with the IPMSM, an experimental laboratory stand with active load unit was realized which allows a simple change of load for testing electrical drive in the static and dynamic states. The active load unit is realized as the vector controlled induction motor drive which allows choosing different load characteristics, for example the load with constant torque, fan and lift characteristics. The control algorithms were realized by microprocessor control system with DSC Freescale 56F8037.

The paper is one of the possibilities of the IPMSM motor vector control and shows the basic advantages and disadvantages of the used IMC method.

The AC drive with the realized speed and current controllers gives good properties in steady state and also in transient states.

REFERENCES

[1] K. B. Bose, *Power Electronics and Modern Electric Drives*. New Jersey: Prentice Hall, 2002.

[2] N. S. Vukosavic, *Digital Control of Electric Drives*. Springer, 2007.

[3] D. Uzel, Z. Peroutka, "Optimal Control and Identification of Model Parameters of Traction Interior Permanent Magnet Synchronous Motor Drive", In *37th Annual Conference of the IEEE Industrial-Electronics-Society (IECON)*, Melbourne, Australia, pp. 1960-1965, 2011.

[4] J. Vittek, P. Bris, P. Makys, M. Stulrajter, "Forced dynamics control of PMSM drives with torsion oscillations", The International Journal for Computation and Mathematics in Electrical and Electronic Engineering COMPEL Vol. 29, Issue 1, pp. 187-204, 2010.

[5] P. Chlebis, P. Moravcik, P. Simonik, "New Method od Direct Torque Control for Three-level Voltage Inverter", In *13th European Conference on Power Electronics and Applications - EPE 2009*, Barcelona, Spain, Vols 1-9, pp. 4051-4056, 2009.

[6] M. J. Duran, T. Glasberger, D. Dujic, E. Levi, Z. Peroutka,"A Modified Sector Based Space Vector PWM Technique for Five-Phase Drives", IEEJ Transactions on Electrical and Electronic Engineering, Vol.4, No.4, pp. 453-464, 2009.

[7] F. J. Gieras, M. Wing, *Permanent Magnet Motor Technology: Design and Applications*. CRC Press, 2002.

[8] R. Krishnan, *Electric Motor Drives: Modeling, Analysis, and Control*. New Jersey: Prentice Hall, 2001.

[9] J. Vittek, S. J. Dodds, *Forced Dynamics Control of Electric Drives*, EDIS - Zilina University, 2003.

[10] L. Jones, J. Lang, "A State Observer for the Permanent-Magnet Synchronous Motor", IEEE Transactions on Industrial Electronics, Vol. 36, pp. 374-382, 1989.

[11] R. Dhaouadi, N. Mohan, L. Norum, "Design and Implementation of an Extended Kalman Filter for the State Estimation of a Permanent Magnet Synchronous Motor", IEEE Transactions on Power Electronics, Vol. 6, pp. 491-497, 1991.

[12] W. Leonhard, *Control of Electrical Drives*. Springer Verlag, 3rd edition, 2001.

[13] T. Tudorache, M. Popescu, "Optimal Design Solutions for Permanent Magnet Synchronous Machines", Advances in Electrical and Computer Engineering Journal, Vol. 11, No. 4, pp. 77-82, 2011. [Online]. Available: http:// dx.doi.org/ 10.4316/AECE.2011.04012

[14] S. Hosseini, J. S. Moghani, B. B. Jensen, "Accurate Modeling of a Transverse Flux Permanent Magnet Generator Using 3D Finite Element Analysis", Advances in Electrical and Computer Engineering Journal, Vol. 11, No. 3, pp. 115-120, 2011. [Online]. Available: http:// dx.doi.org/10.4316/aece.2011.03019

[15] T. Tudorache, I. Trifu, C. Ghita, V. Bostan, "Improved Mathematical Model of PMSM Taking Into Account Cogging Torque Oscillations", Advances in Electrical and Computer Engineering Journal, Vol.12, No 3, pp. 59-64, 2012. [Online]. Available: http:// dx.doi.org/10.4316/ AECE. 2012.03009

[16] O. Wallmark, "Control of Permanent-Magnet Synchronous Machines in Automotive Applications", PhD. Thesis, Chalmers University of Technology, Sweden, 2006.

[17] M. Viteckova, A. Vitecek, *Selected Methods of Adjusting Controllers.* VSB-Technical University of Ostrava, 2011.

[18] P. Vas, *Sensorless Vector and Direct Torque Control*. Oxford University Press, 1998.

[19] P. L. Jansen, R. D. Lorenz, "Transducerless Position and Velocity Estimation in Induction and Salient AC Machines", IEEE Transactions on Industry Applications, Vol. 31, pp. 240-247, 1995.

[20] M. Linke, R. Kennel, J. Holtz, "Sensorless speed and position control of synchronous machines using alternating carrier injection", *IEEE International Electric Machines and Drives Conference - IEMDC'03*, Vol. 2, pp. 1211- 1217, 2003.

[21] D. Saltiveri, A. Arias, G. Asher, M. Sumner, P. Wheeler, L. Empringham, A. C. Silva, "Sensorless Control of Surface Mounted Permanent Magnet Synchronous Motor Using Matrix Converters", Electrical Power Quality and Utilization Journal, Volume X, No. 1, 2006.

[22] Li Yongdong, Zhu Hao, "Sensorless control of permanent magnet synchronous motor - a survey", In *Conference Proceedings of the IEEE Vehicle Power and Propulsion Conference (VPPC)*, Harbin, China, pp. 1-8, 2008.

[23] F. I. Bakhsh, M. Khursheed, S. Ahmad, A. Iqbal, "A novel technique for the design of controller of a vector-controlled permanent magnet synchronous motor drive", In *Conference Proceedings of the 2011 Annual IEEE India Conference - INDICON*, Hyderabad, India, pp. 1-6, 2011.

[24] M. Schroedl, "Sensorless Control of AC Machines at Low Speed and Standstill Based on the "INFORM" Method. In *31st Conference Record of IEEE Industry Applications Conference*, Vol. 1, pp. 270-277, 1996.

[25] T. Krecek, "Sensorless Control of Permanent Magnet Synchronous Motor in the Area of Low Speed", PhD. Thesis, VSB-Technical University of Ostrava, 2009.